Mon. Not. R. Astron. Soc. **000**, 000–000 (0000) Printed 16 August 2007 (MN LATEX style file v2.2)

Submillimetre photometry of X-ray absorbed QSOs: their formation and evolutionary status

J. A. Stevens,[1,2] M. J. Page,[3] R. J. Ivison,[2,4] F. J. Carrera,[5] J. P. D. Mittaz,[6] Ian Smail[7] and I. M. McHardy[8]

[1] *Centre for Astrophysics Research, Science and Technology Research Centre, University of Hertfordshire, College Lane, Herts, AL10 9AB*
[2] *UK Astronomy Technology Centre, Royal Observatory, Blackford Hill, Edinburgh EH9 3HJ*
[3] *Mullard Space Science Laboratory, University College London, Holmbury St. Mary, Dorking, Surrey, RH5 6NT*
[4] *Institute for Astronomy, University of Edinburgh, Royal Observatory, Edinburgh EH9 3HJ*
[5] *Instituto de Fisica de Cantabria (CSIC-UC), Avenida de los Castros 39005 Santander, Spain*
[6] *Department of Physics, University of Alabama in Huntsville, Huntsville, AL 35899, USA*
[7] *Institute for Computational Cosmology, University of Durham, South Road, Durham DH1 3LE*
[8] *Department of Physics and Astronomy, University of Southampton, Southampton, SO17 1BJ*

draft 1.0

ABSTRACT

We present an analysis of the submillimetre/X-ray properties of 19 X-ray absorbed, Compton-thin quasi-stellar objects (QSOs) selected to have luminosities and redshifts which represent the peak of cosmic QSO activity. i.e. $\sim L^*$ objects at $1 < z < 3$. Of these, we present new data for 11 objects not previously observed at submillimetre wavelengths and additional data for a further 3. The detection rate is 42 per cent, much higher than typically reported for samples of QSOs. Detection statistics show (at the $3-4\sigma$ level) that this sample of absorbed QSOs has a higher submillimetre output than a matched sample of unabsorbed QSOs. We argue that the far-infrared luminosity is produced by massive star formation. In this case, the correlation found between far-infrared luminosity and redshift can be interpreted as cosmological evolution of the star-formation rate in the QSO host galaxies. Since the submillimetre luminous phase is confined to $z > 1.5$, the high star formation rates are consistent with a scenario in which the QSOs evolve to become local luminous elliptical galaxies.

Combining these results with previously published data for X-ray unabsorbed QSOs and submillimetre-selected galaxies we propose the following evolutionary sequence: the forming galaxy is initially far-infrared luminous but X-ray weak similar to the sources discovered by the Submillimetre Common-User Bolometer Array; as the black hole and spheroid grow with time a point is reached when the central QSO becomes powerful enough to terminate the star formation and eject the bulk of the fuel supply (the Compton-thin absorbed QSO phase); this transition is followed by a period of unobscured QSO activity which subsequently declines to leave a quiescent spheroidal galaxy.

Key words: galaxies - formation: galaxies - evolution: X-rays - galaxies

1 INTRODUCTION

In the last decade research into active galactic nuclei has moved from the periphery of astrophysics to take centre stage in the study of galaxy formation. This role change was triggered by the discovery that most local spheroidal galaxy components (elliptical galaxies and the bulges of spiral galaxies) contain a massive black hole with mass proportional to that of the velocity dispersion of the stars (Magorrian et al. 1998) or equivalently the mass of the spheroid (e.g. McLure & Dunlop 2002). These relationships suggest a direct link between the growth of the black hole and the stellar mass of the galaxy spheroid.

A second major advance in our knowledge of galaxy formation has occurred in parallel with that involving nuclear activity: the discovery made with the Submillimetre Common-user Bolometer Array (SCUBA; Holland et al. 1999) on the James Clerk Maxwell Telescope (JCMT) of a large population of ultraluminous star-forming galaxies at $z > 1$ (e.g. Smail, Ivison & Blain 1997; Hughes et al. 1998). Semi-analytic models have struggled to reproduce the number counts of these massive galaxies at high redshifts (e.g. Devriendt & Guiderdoni 2000; Baugh et al. 2004) although more recent schemes which include feedback from the active nucleus appear to be more promising (Granato et al. 2004).

E-mail: jas@star.herts.ac.uk

Table 1. Measured redshifts, X-ray fluxes, absorbing column densities and submillimetre flux densities. Also given are the coordinates of the optical QSO.

Source	RA (J2000.0)	Dec (J2000.0)	z	$S_X(\times10^{-14})^a$ (erg cm^{-2} s^{-1})	Log($N_{\rm H}$) (cm^{-2})	S^b_{850} (mJy)	S^b_{450} (mJy)
RX J005734.78 − 272827.4	00 57 34.94	−27 28 28.0	2.19	$1.99^{+0.75}_{-0.56}$	$22.65^{+0.21}_{-0.50}$	11.7 ± 1.2	51 ± 9
RX J033340.22 − 391833.4	03 33 39.54	−39 18 41.4	1.44	$6.68^{+2.63}_{-2.15}$	$22.49^{+0.16}_{-0.41}$	0.9 ± 1.6	...
RX J092103.75 + 621504.3	09 21 02.88	+62 15 06.9	1.46	$5.10^{+1.51}_{-1.31}$	$22.11^{+0.26}_{-0.45}$	0.7 ± 1.4	18 ± 12
RX J094144.51 + 385434.8	09 41 44.61	+38 54 39.1	1.82	$2.98^{+0.91}_{-0.83}$	$21.92^{+0.46}_{-0.42}$	13.4 ± 1.5^c	74 ± 11^c
RX J094356.53 + 164244.1	09 43 57.30	+16 42 49.9	1.92	$8.68^{+4.37}_{-2.91}$	$22.72^{+0.21}_{-0.38}$	3.0 ± 1.2	29 ± 10
XMM J100205.31 + 554258.9	10 02 05.35	+55 42 57.6	1.15	$5.43^{+1.32}_{-1.15}$	$22.84^{+0.18}_{-0.19}$	1.5 ± 0.9	12 ± 8
RX J101033.47 + 533922.5	10 10 33.69	+53 39 29.0	2.46	$2.82^{+1.06}_{-0.77}$	$22.29^{+0.41}_{-0.68}$	-1.6 ± 1.2	-1 ± 9
RX J101112.05 + 554451.3	10 11 12.30	+55 44 47.0	1.25	$8.90^{+1.94}_{-1.31}$	$21.62^{+0.43}_{-0.18}$	2.6 ± 1.0	6 ± 6
RX J101123.17 + 524912.4	10 11 22.67	+52 49 12.3	1.01	$8.67^{+4.35}_{-2.68}$	$22.51^{+0.15}_{-0.29}$	-1.0 ± 1.0^d	-5 ± 9
RX J104723.37 + 540412.6	10 47 23.50	+54 04 06.7	1.50	$2.90^{+1.72}_{-0.99}$	$22.22^{+0.41}_{-0.78}$	1.7 ± 1.1^d	-9 ± 8
RX J110431.75 + 355208.5	11 04 32.44	+35 52 14.1	1.63	$5.43^{+2.65}_{-1.59}$	$22.26^{+0.32}_{-0.68}$	2.4 ± 1.2	29 ± 11
RX J110742.05 + 723236.0	11 07 41.59	+72 32 35.8	2.10	$10.53^{+2.45}_{-1.66}$	$21.58^{+0.82}_{-0.37}$	10.4 ± 1.2	8 ± 9
RX J111942.16 + 211518.1	11 19 42.13	+21 15 16.6	1.29	$4.19^{+0.82}_{-0.68}$	$21.42^{+0.36}_{-0.29}$	-0.5 ± 1.0^d	13 ± 8
RX J121803.82 + 470854.6	12 18 04.54	+47 08 51.0	1.74	$2.36^{+1.15}_{-0.68}$	$22.30^{+0.35}_{-0.56}$	6.8 ± 1.2^e	24 ± 9
RX J124913.86 − 055906.2	12 49 13.85	−05 59 19.4	2.21	$3.39^{+0.85}_{-0.84}$	$22.23^{+0.35}_{-0.63}$	7.2 ± 1.4^e	81 ± 12
XMM J133447.34 + 375950.9	13 34 47.40	+37 59 50.0	1.18	$1.48^{+0.07}_{-0.07}$	$21.83^{+0.06}_{-0.07}$	0.9 ± 1.3	-4 ± 13
RX J135529.59 + 182413.6	13 55 29.54	+18 24 21.3	1.20	$6.25^{+2.84}_{-1.72}$	$22.24^{+0.24}_{-0.50}$	0.8 ± 1.3^e	-8 ± 10
RX J140416.61 + 541618.2	14 04 16.79	+54 16 14.6	1.41	$3.97^{+0.77}_{-0.99}$	$21.69^{+0.39}_{-0.39}$	0.1 ± 1.1	11 ± 12
RX J163308.57 + 570258.7	16 33 08.59	+57 02 54.8	2.80	$2.66^{+0.74}_{-0.58}$	$22.47^{+0.32}_{-0.48}$	5.9 ± 1.1^e	9 ± 9

[a] Absorption corrected $0.5 - 2$ keV X-ray flux
[b] Quoted errors do not include calibration uncertainties (see Section 2)
[c] Flux densities from Stevens et al. (2004). The quoted 450 μm value corresponds to emission from source 1 and 2 in that paper.
[d] New data combined with those from Page et al. (2001)
[e] From Page et al. (2001)

There are two obvious direct approaches that can be taken to investigate the coupled formation of a galactic bulge and its black hole. One is to make X-ray observations of known submillimetre-bright galaxies. The first experiments showed little overlap between the two populations (Fabian et al. 2000). However, once more sensitive X-ray observations became available many SCUBA-selected galaxies were found to have weak X-ray counterparts (Alexander et al. 2003, 2004). From these data, it can be concluded that the major episode of star formation does not coincide with the epoch of visible quasi-stellar object (QSO) activity although an evolutionary link between SCUBA-selected galaxies and QSOs may still exist (e.g. Almaini 2003).

The second approach is that taken here: to select typical AGN at X-ray wavelengths, i.e. those responsible for the majority of the comoving accretion luminosity density, and observe them at submillimetre wavelengths (Page et al. 2001). To date we have observed two matched samples of X-ray selected QSOs. The first of these comprised 8 QSOs showing strong evidence for photoelectric absorption in their X-ray spectra – indicating the presence of gas in the line-of-sight to the nucleus. Of these, the 4 at $z > 1.5$ were detected as ultraluminous or hyperluminous far-infrared galaxies while the 4 at $z < 1.5$ were not. We argued that these results were consistent with the coeval growth of the galaxy spheroid and black hole in these systems (Page et al. 2001) but that, with the available data, it was not possible to determine whether the redshift trend could be attributed to cosmological evolution or selection effects. The second sample comprised 20 objects that showed no evidence for photoelectric absorption; these have properties akin to the majority of QSOs selected at optical wavelengths. Only one of these QSOs was detected by SCUBA with $> 3\sigma$ significance (Page et al. 2004).

This striking result indicates that the absorption in these objects is not a consequence of the basic 'unified scheme' (Antonucci 1993) in which the X-ray properties of QSOs are determined by viewing angle alone. Instead it can be argued that the absorbed QSOs are transition objects caught between an epoch of hidden growth and an unobscured QSO phase, and that the absorbed phase coincides with the formation of the galaxy spheroid (Page et al. 2004).

The motivation for the present study is straightforward: X-ray absorbed QSOs selected by our criteria must be important objects in the history of galaxy formation but only 8 objects have been observed at submillimetre wavelengths. Here we report sensitive submillimetre observations of another 11 objects making the sample sufficiently large to (1) improve the detection statistics, and (2) search for trends between submillimetre and X-ray properties. A Hubble constant $H_0 = 70$ km s^{-1} Mpc^{-1} and density parameters $\Omega_\Lambda = 0.7$ and $\Omega_{\rm m} = 0.3$ are assumed throughout.

2 SAMPLE SELECTION, OBSERVATIONS AND DATA REDUCTION

We selected X-ray absorbed QSOs from the *Rosat* sample of Page, Mittaz & Carrera (2001) and from the new generation of surveys being conducted with *XMM-Newton* and *Chandra* (e.g. Page et al. 2003; McHardy et al. 2003). They are selected to (1) span the redshift range $1 < z < 3$ and (2) have $0.5 - 2$ keV X-ray luminosities $\sim 1 - 10\ L^*_{\rm X}$ where $L^*_{\rm X}$ is the break in the X-ray luminosity function measured in erg s^{-1} and has values $44.1 < {\rm Log}(L^*_{\rm X}) < 44.4$ for $1 < z < 3$ (e.g. Page et al 2004). They are thus typical objects selected at the peak of QSO activity. The QSOs are all Comp-

Table 2. X-ray and far-infrared luminosities calculated from the data presented in Table 1. We also give the ratio of far-infrared luminosity to bolometric luminosity of the QSO (see text for details) and to $0.5-2.0$ keV X-ray luminosity.

Source	Log(L_X) (erg s^{-1})	Log($L_{\rm FIR}$) ($L_\odot$)	($L_{\rm FIR}/L_{\rm QSO}$)	($L_{\rm FIR}/L_{\rm X}$)
RX J005734.78 − 272827.4	$44.85^{+0.14}_{-0.14}$	$13.32^{+0.08}_{-0.06}$	3.4 ± 1.4	114 ± 47
RX J033340.22 − 391833.4	$44.93^{+0.15}_{-0.17}$	< 12.90	< 1.1	< 36
RX J092103.75 + 621504.3	$44.83^{+0.11}_{-0.13}$	< 12.84	< 1.2	< 39
RX J094144.51 + 385434.8	$44.83^{+0.12}_{-0.14}$	$13.41^{+0.05}_{-0.07}$	4.8 ± 1.8	146 ± 55
RX J094356.53 + 164244.1	$45.36^{+0.17}_{-0.18}$	$12.76^{+0.13}_{-0.22}$	0.3 ± 0.2	10 ± 7
XMM J100205.31 + 554258.9	$44.61^{+0.09}_{-0.11}$	< 12.79	< 1.7	< 58
RX J101033.47 + 533922.5	$45.13^{+0.14}_{-0.14}$	< 12.80	< 0.5	< 18
RX J101112.05 + 554451.3	$44.90^{+0.09}_{-0.06}$	< 12.92	< 1.2	< 40
RX J101123.17 + 524912.4	$44.67^{+0.18}_{-0.16}$	< 12.53	< 0.8	< 28
RX J104723.37 + 540412.6	$44.62^{+0.20}_{-0.18}$	< 12.86	< 2.0	< 69
RX J110431.75 + 355208.5	$44.98^{+0.17}_{-0.15}$	$12.65^{+0.18}_{-0.30}$	0.5 ± 0.4	18 ± 16
RX J110742.05 + 723236.0	$45.54^{+0.09}_{-0.08}$	$13.28^{+0.06}_{-0.08}$	0.6 ± 0.2	21 ± 6
RX J111942.16 + 211518.1	$44.61^{+0.08}_{-0.07}$	< 12.56	< 1.0	< 34
RX J121803.82 + 470854.6	$44.69^{+0.17}_{-0.15}$	$13.10^{+0.08}_{-0.10}$	3.0 ± 1.5	99 ± 50
RXJ J124913.86 − 055906.2	$45.10^{+0.10}_{-0.13}$	$13.11^{+0.09}_{-0.11}$	1.2 ± 0.5	39 ± 7
XMM J133447.34 + 375950.9	$43.97^{+0.02}_{-0.03}$	< 12.80	< 7.8	< 260
RX J135529.59 + 182413.6	$44.71^{+0.16}_{-0.14}$	< 12.79	< 1.4	< 46
RX J140416.61 + 541618.2	$44.68^{+0.08}_{-0.12}$	< 12.63	< 1.0	< 34
RX J163308.57 + 570258.7	$45.24^{+0.11}_{-0.10}$	$13.00^{+0.08}_{-0.11}$	0.7 ± 0.2	22 ± 3

ton thin with absorbing column densities measured in cm^{-2} of $21 < \mathrm{Log}(N_{\rm H}) < 23$ and have broad optical emission lines.

For the *Rosat*-selected QSOs, column densities were determined by fitting an absorbed power law to a three-band *Rosat* PSPC spectrum. The source and background counts, which were determined from images constructed in the three energy bands, are given in table 2 of Page, Mittaz & Carrera (2000). The three energy bands correspond to PSPC PI channels $11-41$, $52-90$, and $91-201$. The mean X-ray power-law spectral index of unabsorbed QSOs is $\alpha = 1$ (where $f_\nu \propto \nu^{-\alpha}$), with a standard deviation of ~ 0.2 (Page et al. 2003; Mateos et al. 2005). Therefore we assumed a power-law index $\alpha = 1$ and included a fixed component of Galactic absorption in the fit. The power-law normalization and the column density of a cold absorber at the redshift of the QSO were free parameters in the fit, which was performed using the Cash statistic C (Cash 1979). Uncertainties on the fit parameters were obtained first by constructing two-dimensional ΔC contours and then marginalised by integrating over one of the parameters, as described in Mittaz et al. (1999). This is identical to the method used by Page, Mittaz & Carrera (2001).

For the two *XMM-Newton*-selected QSOs, X-ray spectra were constructed from EPIC *pn* (Strüder et al. 2001) and MOS (Turner et al. 2001) data. The data were reduced using the *XMM-Newton* Science Analysis System (SAS) V6.0. Source counts were obtained from elliptical spatial regions, oriented to match the off-axis *XMM-Newton* point spread function. Background counts were obtained from an annular region surrounding the source, with bright sources excised. Response matrices and effective area files were constructed using the appropriate SAS tasks. For each source, the MOS and *pn* spectra were then combined and suitable background and response files were constructed using the method of Page, Davis & Salvi (2003). Finally, the spectra of XMM J100205 + 554258.9 and XMM J133447 + 375950.9 were grouped to minima of 16 and 30 counts per bin respectively before χ^2 fitting. Both objects are viewed through extremely low Galactic absorbing columns of 8×10^{19} cm^{-2}. However, XMM J100205+554258.9 lies behind an additional line of sight column density of 4.8×10^{20} cm^{-2} which is associated with NGC 3079 (Womble, Junkkarinen & Burbidge 1992), and so for this object we set the Galactic column density to 5.6×10^{20} cm^{-2} in the spectral fit. The X-ray spectrum of XMM J100205 + 554258.9 is acceptibly fitted ($\chi^2/\nu = 6.5/4$) with the same model as used for the *Rosat* QSOs (i.e. an absorbed power law with fixed $\alpha = 1$). XMM J133447+375950.9, however, is not well fitted by this model. Instead, allowing a slightly harder continuum slope of $\alpha = 0.7$ (still within the range commonly observed in unabsorbed AGN) results in an acceptable $\chi^2/\nu = 45/39$. The two *XMM-Newton* spectra are shown in Fig. 1. Names, optical coordinates, redshifts, X-ray fluxes and absorbing column densities are listed in Table 1.

Submillimetre photometry observations at 450 and 850 μm were performed at the JCMT during 2003 December and 2004 January. We used SCUBA in standard 2-bolometer chopping mode which allows a second bolometer on each array to sample the source position in one half of the nod cycle giving a $(4/3)^{1/2}$ reduction in the noise compared to 1-bolometer mode. Data were taken simultaneously at 450 and 850 μm in ~ 1 hour blocks separated by pointing checks on a near-by blazar and focus checks as appropriate. The sky opacity was monitored on a quasi-continuous basis with the JCMT water vapour radiometer and cross-checked with skydips about twice per night. Flux density calibration was made against Uranus or the compact secondary calibrator CRL 618 (Sandell 1994; Jenness et al. 2002). Calibration uncertainties are about 10 and $15-20$ per cent at 850 and 450 μm respectively. We aimed for a uniform noise level of ~ 1 mJy at 850 μm thus allowing a proper statistical analysis of the submillimetre properties. For this reason we re-observed 3 sources previously reported by Page et al. (2001). Observations were made in good-to-excellent conditions with the 225 GHz opacity as measured at the adjacent Caltech Sub-

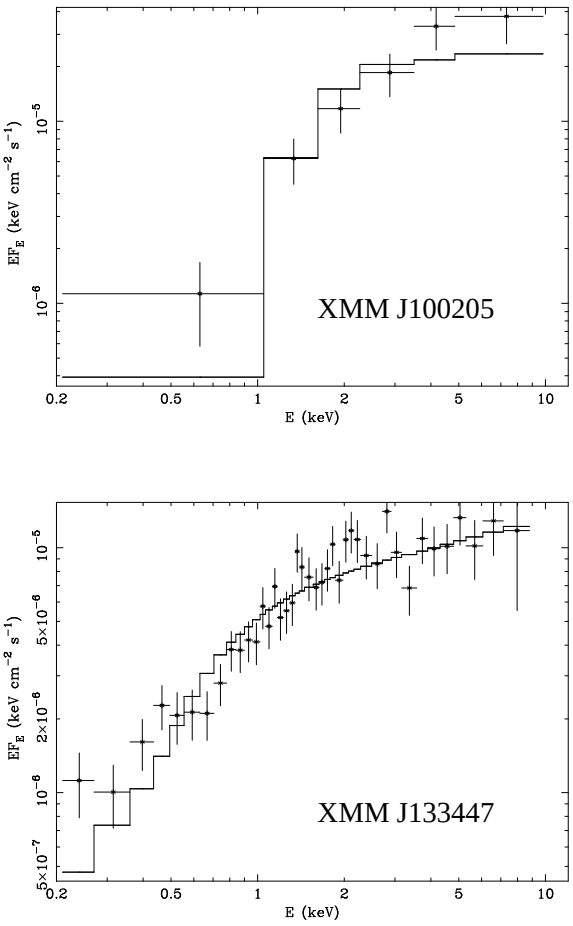

Figure 1. The *XMM-Newton* spectra of XMM J100205 + 554258.9 (top) and XMM J133447 + 375950.9 (bottom) along with the best-fitting absorbed power-law models (stepped lines). The *XMM-Newton* effective area has been divided out of both model and data in these plots.

millimeter Observatory always < 0.08. During the best weather we made 6 detections at 450 μm with signal-to-noise (S/N) greater than or approximately 3.

Data were reduced with the STARLINK SURF package in the standard manner (see e.g. Holland et al. 1999). We reduced data from different nights and with different bolometers separately and calculated a weighted mean flux density and error. The final photometry results are listed in Table 1.

3 RESULTS

3.1 Luminosities

In Table 2 we present X-ray and far-infrared luminosities for each source. The 850-μm flux densities are converted into far-infrared luminosites ($L_{\rm FIR}$) by scaling them with that of Mrk 231 which is a local ultraluminous infrared galaxy (ULIRG) hosting an X-ray absorbed QSO; we calculate $L_{\rm FIR} = 1.9 \times 10^{12}$ L$_\odot$ by modelling its millimetre–far-infrared spectral energy distribution. Quoted uncertainties on $L_{\rm FIR}$ are calculated by adding in quadrature the error given in Table 1 with the estimated 10 per cent calibration uncertainty. Note that the uncertainties will be under-estimates unless the QSOs have the same spectrum as Mrk 231. For example, if we used Arp 220 or Mrk 273 as templates then calculated values of $L_{\rm FIR}$ would be systematically lower by factors of 1.5 and 1.6 respectively. However, we stress that the choice of template only affects the normalization of the derived luminosities; its variation as a function of redshift over the range covered by our sources is small for all realistic templates because the strong negative K-correction at 850 μm cancels out the effect of cosmological dimming (e.g. Blain & Longair 1993). The template producing the smallest variation in flux density between $1.0 < z < 2.8$ is Mrk 231 (~ 1 per cent) whilst the largest variation (~ 20 per cent) comes from Arp 220. The maximum scatter introduced by this effect is thus roughly comparable to the estimated uncertainties (~ 0.1 dex) on the computed luminosities and will not affect our conclusions. Upper limits to $L_{\rm FIR}$ are calculated from the 850-μm flux densities (S_{850}) using values ($2\sigma + S_{850}$) if $S_{850} > 0$ and 2σ if $S_{850} < 0$. Bolometric luminosities for the QSOs are calculated assuming that 3 per cent of the bolometric output of the AGN is emitted in the $0.5 - 2.0$ keV band (Elvis et al. 1994). Note that these bolometric luminosities are computed from the rest frame spectral energy distributions of the QSOs and include data ranging from radio to hard X-ray wavelengths. They thus include contributions from the direct AGN continuum and reprocessed emission that emerges at longer wavelengths.

3.2 Detection statistics and comparison with other samples

With this sample of 19 sources we can place better statistical constraints on the prevalence of luminous star formation in the absorbed QSO population than was possible in our previous study which contained 8 sources (Page et al. 2001). Throughout this paper two sources with $2 < ({\rm S/N}) < 3$ in both wavebands are treated as detections: RX J094356.53 + 164244.1 and RX J110431.75 + 355208.5. Both of these objects have higher S/N at 450 μm than at 850 μm which is quite common for thermal sources observed in excellent weather conditions. We consider these sources to be 'submillimetre detections' and use their 850-μm flux densities in subsequent analysis. A third QSO, RX J101112.05 + 554451.3 is marginally 'detected' at 850 μm (2.6σ) but not at 450 μm. We do not consider this source as a detection but note that its inclusion as such would not alter the interpretation of the correlation results presented in Section 3.3. The other 6 detections are all at $> 5\sigma$ significance at 850 μm. As found for the smaller sample, the detection rate is high (42 per cent) at 850 μm. The weighted mean flux density of the complete sample is 3.1 ± 0.3 mJy. The detected and non-detected subsamples have weighted means of 7.3 ± 0.4 and 0.6 ± 0.3 mJy respectively.

Two of the QSOs are radio loud: RX J110431.75 + 355208.5 and RX J163308.57 + 570258.7. Both of these objects were detected at submillimetre wavelengths so we need to consider whether the 850 μm emission could be due to synchrotron radiation rather than reprocessed thermal emission. The case of RX J163308.57 + 570258.7 was discussed by Page et al. (2001) who extrapolated its radio spectrum assuming a power-law and found an insignificant synchrotron contribution of < 0.1 mJy at 850 μm. For RX J110431.75 + 355208.5 the Very Large Array FIRST survey gives an integrated 1.4-GHz flux density of 71.5 mJy while the Westerbork Northern Sky Survey gives an integrated 325-MHz flux density of 298 mJy. A naive power-law extrapolation of these measurements gives ~ 0.3 mJy at 850 μm. A synchrotron contribution at 850 μm cannot thus be ruled out, although the thermal emission is likely to be a much more significant component. Given the

Table 3. Correlation probabilities from the survival analysis tests. Quoted values give the probability that a correlation is present between the two parameters.

Sample	Test	$P(L_{\rm X}, z)$	$P(L_{\rm FIR}, z)$	$P(L_{\rm FIR}, L_{\rm X})$	$P(L_{\rm FIR}, N_{\rm H})$
Full ($n = 19$)	Cox hazard	0.997	0.998	0.979	0.653
	Kendall's tau	> 0.999	0.995	0.917	0.233
Restricted ($n = 13$)	Cox hazard	0.727	> 0.999	0.813	0.558
	Kendall's tau	0.889	0.995	0.635	0.488

uncertainties we do not apply a correction and assume that the submillimetre radiation is thermal emission from warm dust.

This sample contains a significantly higher proportion of detections than a similarly selected sample of unabsorbed QSOs in which we detected only 1 object in 20 (5 per cent) with $> 3\sigma$ significance (Page et al. 2004). Note that each QSO in this unabsorbed sample was observed down to the same ~ 1 mJy flux density limit as the absorbed sample and none of them would qualify as a 'submillimetre detection' based on their combined 850- and 450-μm photometry. The resulting weighted mean 850-μm flux density of these 20 unabsorbed QSOs was found to be only 0.7 ± 0.2 mJy. Similarly, in a $z \sim 2$ optically selected sample of very high luminosity ($> 20L^*$) QSOs only 9 out of 57 objects (16 per cent) were detected with $> 3\sigma$ significance (Priddey et al. 2003). Although these latter submillimetre observations were relatively shallow (the median rms flux density was ~ 2.8 mJy), the weighted mean flux density of the undetected sources was only 1.9 ± 0.4 mJy, insufficiently high to rule out AGN heating as the power source of the submillimetre dust emission (Priddey et al. 2003). These values are consistent with those found from stacking the submillimetre flux density at the positions of faint X-ray sources detected by *Chandra* and *XMM-Newton*. For the former, Barger et al. (2001) found a noise-weighted mean 850-μm flux density of 1.2 ± 0.3 mJy while Almaini et al. (2001) found 0.9 ± 0.3 mJy. For the latter, Waskett et al. (2003) report $\sim 0.4 \pm 0.3$ mJy.

By contrast, in the present sample we detected 8 out of 19 QSOs. The Bayesian posterior probability of getting n sources showing a given property out of a sample of N sources is

$$P(f) \propto (f + f_{spu})^n (1 - f - f_{spu})^{(N-n)}$$

where f is the fraction of the underlying population showing that property, and f_{spu} the fraction of spurious detections (in the case of 3σ detections $f_{spu} = 0.0027 \equiv 1 - 0.9973$). This $P(f)$ can be normalized integrating over f between 0 and 1; we have assumed here a diffuse prior, meaning that the a priori probability of f is flat between 0 and 1. As intuitively expected, $P(f)$ peaks at $\sim n/N - f_{spu}$, and confidence intervals can be obtained integrating it around that peak to the desired confidence level. For the X-ray absorbed QSOs presented here ($n = 8$ and $N = 19$) between 19 and 61 per cent of the population from which they are selected will be detected at 850 μm with a flux density $> 2-3$ mJy at 95 per cent confidence. For the matched sample of unabsorbed QSO presented in Page et al. (2004) ($n = 1$ and $N = 20$) less than ~ 21 per cent of the objects will present that level of emission.

This formalism can also be used to compare two samples. Under the null hypothesis that both samples are drawn from the same underlying population, in which a fraction f of sources are detectable in the submillimetre band,

$$P(f) \propto (f + f_{spu})^{(n+m)} (1 - f - f_{spu})^{(N+M-n-m)}$$

where again n sources are detected out of N in one sample, and m out of M in a second independent sample. Given this $P(f)$, if we draw from the total population two independent samples of sizes N and M, respectively, the probability $P(i, j; N, M)$ of detecting i sources in the first sample, and j in the second is given by

$$\begin{aligned} P(i,j;N,M) &= \left(\frac{N}{i}\right)\left(\frac{M}{j}\right)\int_0^1 df\, P(f)\,(f + f_{spu})^{(i+j)} \\ &\times \quad (1 - f - f_{spu})^{(N+M-i-j)}. \end{aligned}$$

Finally, two samples are significantly different if the probability of detecting $\geq n$ sources in the first sample and $\leq m$ sources in the second ($P(\geq n, \leq m; N, M) = \sum_{i=n}^{N} \sum_{j=0}^{m} P(i, j; N, M)$) is smaller than a chosen significance. We find $P(\geq 8, \leq 1; 19, 20) = 0.0014$, which means that our matched samples of X-ray absorbed and unabsorbed AGN are different at $> 3\sigma$ significance. If we consider the $z > 1.5$ samples only, we find $P(\geq 8, \leq 1; 10, 12) = 5.6 \times 10^{-5}$ ($> 4\sigma$ significance).

3.3 Correlation analysis

We would like to know whether $L_{\rm FIR}$ is correlated with redshift (z), X-ray luminosity ($L_{\rm X}$) or absorbing column density ($N_{\rm H}$). These quantities are plotted against each other in Fig. 2. Since our dataset contains a large fraction of upper limits we have to use 'survival analysis' techniques (e.g. Isobe, Feigelson & Nelson 1986). The most appropriate tests are those performed by the Cox proportional hazard model and the Generalized Kendall's tau. Spearman's rank order test which is known to be unreliable for datasets of < 30 points is not used. The two adopted tests are suitable for datasets in which the dependent variable (in our case $L_{\rm FIR}$) contains only one kind of censoring (in our case upper limits).

Using the IRAF tasks COXHAZARD and BHKMETHOD we tested for correlations between $L_{\rm FIR}$ and z, $L_{\rm X}$ and $N_{\rm H}$ in the full sample of 19 QSOs. The correlation probabilities are given in Table 3. Note that although the adopted correlation tests return the probability Q that a correlation is not present, the quoted values $P = 1 - Q$ give the probability of the opposite outcome. Both tests return high probabilities for a correlation between $L_{\rm FIR}$ and z and low probabilities for a correlation between $L_{\rm FIR}$ and $N_{\rm H}$. However, they both return a reasonably high likelihood that $L_{\rm FIR}$ is correlated with $L_{\rm X}$. In this case we must test whether $L_{\rm X}$ correlates with z since a trend between $L_{\rm FIR}$ and $L_{\rm X}$ could result from a mutual correlation with z. Table 3 shows that both tests return a high probability that $L_{\rm X}$ and z are correlated.

For the full sample of 19 QSOs this analysis shows that we cannot determine whether $L_{\rm FIR}$ correlates with $L_{\rm X}$ or with z. However, when selecting the QSOs we endeavoured to minimize any correlation between $L_{\rm X}$ and z which allows us to select a sizable subsample for which these two parameters are uncorrelated. Thus we can restrict the sample to comprise those 13 objects satisfying $44.5 \leq {\rm Log}(L_{\rm X}) \leq 45.0$. The correlation analysis for this restricted sample is also given in Table 3 and we plot $L_{\rm X}$ vs z, $L_{\rm FIR}$ vs z and $L_{\rm FIR}$ vs $L_{\rm X}$ in Fig. 3. For these 13 QSOs there is now no

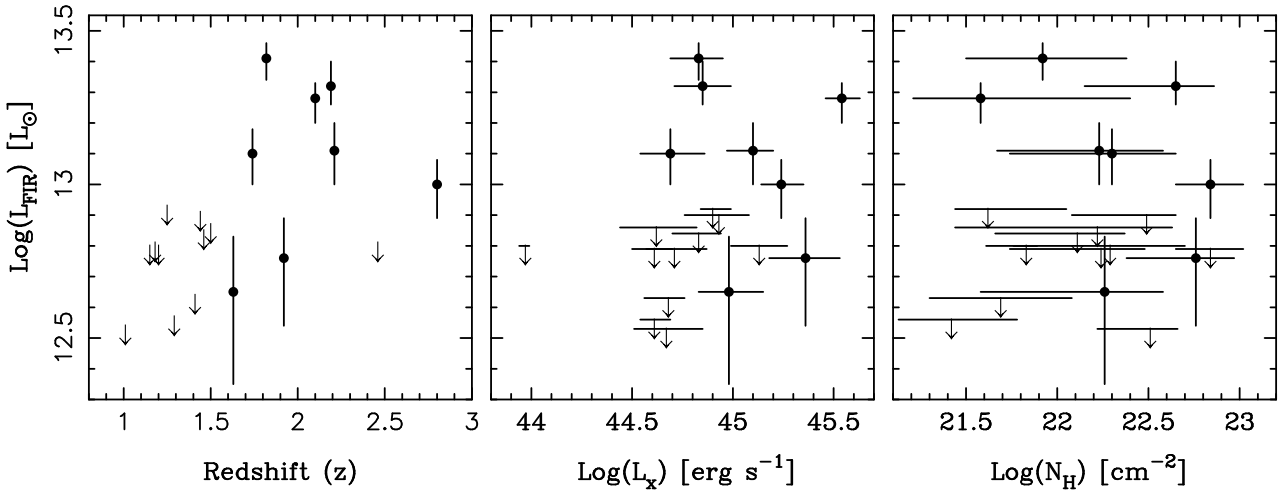

Figure 2. The panels (from left to right) show far-infrared luminosity ($L_{\rm FIR}$) versus redshift, $0.5-2.0$ keV X-ray luminosity ($L_{\rm X}$) and X-ray absorbing column density ($N_{\rm H}$).

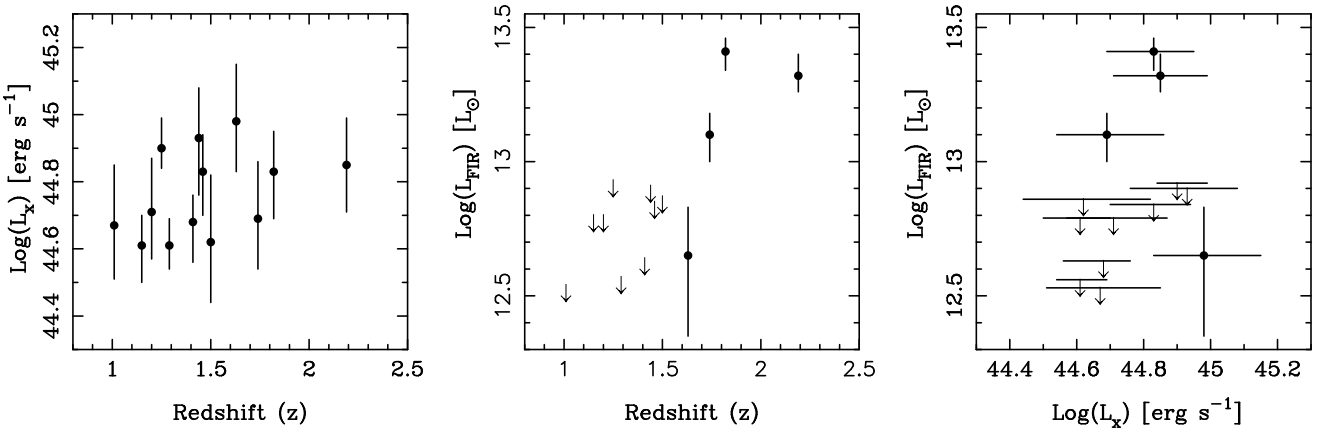

Figure 3. The panels (from left to right) show X-ray luminosity ($L_{\rm X}$) versus redshift, far-infrared luminosity ($L_{\rm FIR}$) vs redshift, and X-ray luminosity vs far-infrared luminosity for the sample of QSOs restricted to have $44.5 \leq {\rm Log(L_X)} \leq 45.0$. The only significant correlation is between $L_{\rm FIR}$ and redshift (see text for details).

correlation between $L_{\rm X}$ and z or between $L_{\rm X}$ and $L_{\rm FIR}$, but both tests give a strong correlation between $L_{\rm FIR}$ and z. We note that the resticted range in $L_{\rm X}$ makes the analysis insensitive to any real correlation between $L_{\rm FIR}$ and $L_{\rm X}$; this is not the right sample to search for such a correlation. However, the analysis does show that the correlation between $L_{\rm FIR}$ and z is real, i.e. it does not result from a mutual correlation with $L_{\rm X}$. We discuss the implications of this correlation in Section 4.

3.4 The power source of the far-infrared emission

It has already been argued that the intrinsic difference between the submillimetre properties of absorbed and unabsorbed QSOs suggests that the former are undergoing major starbursts (see Page et al. 2004 and Section 1). For completeness we should also consider the viability of the alternative scenario in which the AGN heats the dust. In this case, the observed dichotomy in far-infrared luminosity must be related to an intrinsic difference in the circumnuclear environment of the two types of QSOs. We note, however, that such an interpretation appears somewhat ad hoc since it is not obviously apparent what the physical explanation for such a difference would be (although see Barger et al. 2005). Nevertheless, such a possibility is considered below.

We first consider the diagnostic used by Page et al. (2001), namely the ratio of far-infrared luminosity to bolometric output of the QSO. These values are listed for each QSO in Table 2. In

three cases the measured far-infrared luminosities are significantly greater than the entire bolometric output of the QSO, and in most other cases comprise a sizable fraction of it. For the former cases the QSO cannot possibly power the far-infrared luminosity. For the latter, the QSO can only power the far-infrared emission if the majority of the QSO emission is absorbed and reprocessed by dust. Since we observe these QSOs to be relatively unattenuated in the rest-frame ultraviolet, it also appears unlikely that they are the dominant power sources for the far-infrared dust emission.

It is also instructive to compare the far-infrared/X-ray output of our QSOs with that of the $0 < z < 1$ UVSX quasars presented by Elvis et al. (1994). These are 'normal' optically bright quasars that were detected in the X-ray band by *Einstein*. We first removed from the sample objects classified as flat-spectrum compact, steep spectrum compact or Fanaroff-Riley class 2 steep spectrum doubles. Since the output from these objects is likely contaminated by non-thermal emission they are not good lower-redshift analogues of our QSOs. Far-infrared luminosities were calculated for the remaining 34 quasars by scaling their 60-μm flux densities with that of IZw 1 (PG 0050+124), one of the UVSX quasars with flux density measurements at far-infrared through submillimetre wavelengths (Hughes et al. 1993; Haas et al. 2000). We fitted its spectrum with an isothermal greybody giving a far-infrared luminosity of 3.3×10^{11} L$_\odot$. The $0.1 - 1.0$ keV X-ray luminosities from Elvis et al. (1994) were converted to our adopted cosmology and corrected to $0.5 - 2.0$ keV luminosities assuming a photon index, $\Gamma = 2.0$.

We plot the histogram of $L_{\rm FIR}/L_{\rm X}$ in Fig. 4 (lower panel) and show for comparison (upper panel) the histogram of values for our SCUBA-detected absorbed QSOs (Table 2). While the number of absorbed QSOs is small, the two histograms are clearly different. The UVSX quasars have values that peak strongly (30/34 cases) in the first two bins ($L_{\rm FIR}/L_{\rm X} < 10$) while the absorbed QSOs have values ranging between ~ 10 and 150. If we assume that the X-rays are produced close to the central engine by the same mechanism for all quasars then this result suggests that the far-infrared emission does not have the same origin in the two samples. For the UVSX quasars, the $L_{\rm FIR}/L_{\rm X}$ values have a small scatter – the 60-μm detected sources have a mean value of 5 ± 5 – suggesting that the far-infrared luminosity is physically related to the output of the AGN. Indeed, the survival analysis tasks BHKMETHOD and COXHAZARD return correlation probabilities of > 0.999 and 0.999 respectively. An obvious interpretation is that the far-infrared emission is reprocessed quasar continuum, possibly from dust in a circumnuclear torus. For the absorbed QSOs the excess far-infrared luminosity can be attributed to dust heated by hot young stars.

In addition, we note that recent submillimetre imaging results for one of the absorbed QSOs show dust emission extended over tens of kpc in an apparent merger morphology (Stevens et al. 2004). Similar observations of high-redshift radio galaxies often yield the same result (Stevens et al. 2003). For the submillimetre-detected absorbed QSOs we conclude that all available evidence points towards dust heated in a major starburst rather than by an AGN continuum.

Finally, let us consider the submillimetre non-detected absorbed QSOs. In Section 3.2 we found that the mean flux density of these objects is 0.6 ± 0.3 mJy. Scaling with IZw 1 which has a predicted 850-μm flux density of $0.34 - 0.39$ mJy over the relevant redshift range ($1.0 < z < 1.5$) gives a mean far-infrared luminosity of $\sim 6 \pm 3 \times 10^{11}$ L$_\odot$. The mean X-ray luminosity for these objects using the values from Table 2 is $5.0^{+4.4}_{-2.4} \times 10^{44}$ erg s^{-1}. Thus the mean value of $L_{\rm FIR}/L_{\rm X} \sim 4 \pm 4$ for the non-detected absorbed QSOs is wholly consistent with the mean value found for the UVSX quasars suggesting that they may have similar properties.

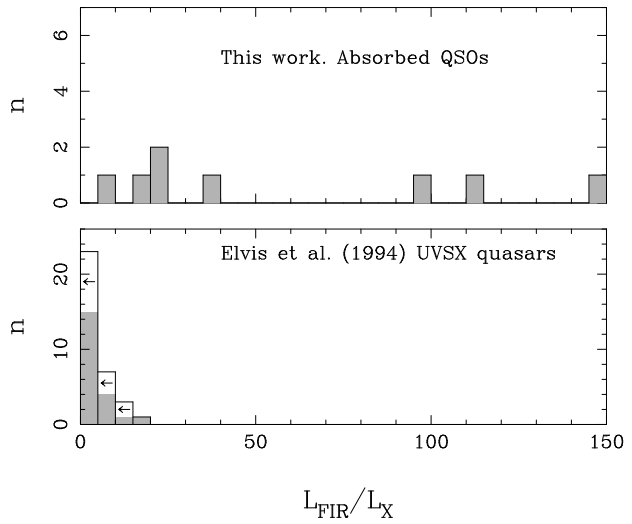

Figure 4. Histograms of the ratio of far-infrared luminosity to X-ray luminosity for (top panel) SCUBA detected absorbed QSOs from this work and (bottom panel) UVSX quasars from Elvis et al. (1994). On the bottom panel shaded regions show the number of detections in each bin while unshaded regions with arrows show lower limits.

4 INTERPRETATION: AN EVOLUTIONARY SEQUENCE?

In the previous section it was argued that the submillimetre emission from SCUBA-detected absorbed QSOs can be attributed to dust heated by hot young stars. In this case, the implied star-formation rates, given by $\mathrm{SFR}(\mathrm{M}_\odot\,\mathrm{yr}^{-1}) = L_{\rm FIR}/(5.8\times10^9\mathrm{L}_\odot)$ (Kennicutt 1998) are > 1000 M$_\odot$ yr^{-1}, sufficiently high to build a substantial fraction of a galaxy spheroid in only a few 100 Myr. In Page et al. (2004) we argued (1) that their space density relative to unabsorbed QSOs indicates that the absorbed phase has a duration ~ 15 per cent that of the unabsorbed phase (2) that unabsorbed QSOs have already built most of their stellar mass implying that the absorbed phase precedes the epoch of luminous unobscured QSO activity (3) that the X-ray luminosities of the absorbed sources imply that they contain black holes of mass $> 10^8$ M$_\odot$. The conclusion of that work was thus that absorbed QSOs are observed during a transition phase between their highly-obscured growth and a period of unabsorbed QSO activity.

The analysis of a larger sample of absorbed QSOs presented here strengthens these claims. In particular, we have shown statistically that absorbed QSOs have higher submillimetre flux densities than unabsorbed QSOs of given X-ray luminosity and redshift. Their submillimetre detection rate is also much higher than luminous QSOs selected at optical wavelengths. In addition, for the restricted sample, we find evidence that X-ray absorbed QSOs were forming stars much more rapidly at early epochs. All 8 QSOs detected at submillimetre wavelengths lie at $z > 1.5$. This result indicates cosmological evolution of the star-formation rate density in the absorbed QSO population. A similar result was found for radio galaxies (Archibald et al. 2001; Reuland et al. 2004) although these have a much lower space density than $\sim L_{\rm X}^*$ QSOs. Such an

early epoch of copious star formation is consistent with these QSOs evolving to become elliptical galaxies at lower redshifts. Indeed, at $0 < z < 0.5$ we know that elliptical galaxies are preferentially found in cluster environments where they have old, coeval stellar populations. The small intrinsic scatter in the colours of ellipticals within these clusters suggests that they formed the bulk of their stars synchronously at $z > 2$ or so (Ellis et al. 1997). This result is explained naturally by the hierarchical model of galaxy formation since density peaks on galaxy scales collapse, on average, at higher redshifts if they are situated in large-scale over densities. Such over-dense regions evolve to form a cluster at $z = 0$ (Kauffmann 1996).

We can compare our proposed evolutionary sequence for QSOs with the physical model presented by Granato et al. (2004) who consider joint spheroid/QSO evolution within a hierarchical clustering scenario (although see Baugh et al. 2004 who discuss some of the assumed simplifications). Their model, which is able to reproduce the SCUBA number counts, makes a number of predictions that are in good accord with the results presented here and by Page et al. (2004). It predicts that the luminous starburst phase begins before the black hole has built sufficient mass to shine as a luminous QSO, but that this starburst is still ongoing, with a $\mathrm{SFR} > 1000\ \mathrm{M_{\odot}yr^{-1}}$, as the black hole reaches its final mass of $10^8 - 10^9\ \mathrm{M_{\odot}}$ (for a $10^{12.4} - 10^{13.4}\ \mathrm{M_{\odot}}$ dark matter halo). Sources caught in this phase would have properties commensurate with those of our $z > 1.5$ X-ray absorbed QSOs. During this transition the quasar feedback removes most of the gas and dust leaving the nucleus shining as an unabsorbed/optically-selected QSO (see also Silk & Rees 1998; Fabian 1999; Di Matteo, Springel & Hernquist 2005) – consistent with the lack of evidence for substantial star formation in such objects discussed earlier. Sources caught during the initial luminous starburst phase may comprise the bulk of the submillimetre galaxy population discovered with SCUBA (Smail, Ivison & Blain 1997) – many are ULIRGs containing growing black holes with Seyfert-like X-ray luminosities (Alexander et al. 2003; Smail et al. 2003; Alexander et al. 2004) and they often show signatures of buried AGN in their optical spectra (Chapman et al. 2003, 2004).

Where do the $z < 1.5$ absorbed QSOs fit into this scheme? None of these objects are luminous submillimetre sources. One possibility is that the absorption in the $z < 1.5$ objects arises in an obscuring circumnuclear torus whereas at $z > 1.5$ it is related to the major formation epoch of the stellar spheroid. Such a possibility, while plausible, is a little contrived. A second, and maybe more natural explanation, might be that fuelling of the AGN/starbursts evolves with redshift (as already alluded to above). At high redshifts, merger events or interactions that trigger the activity occur between gas-rich galaxies (e.g. Kauffmann & Haehnelt 2000), producing luminous starbursts and obscured X-ray sources. However, at lower redshifts, while the QSO may undergo recurrent merger induced accretion episodes that drive enough gas into the nuclear region to produce the observed X-ray absorption, there is insufficient fuel for them to be accompanied by starbursts luminous enough to be detected by SCUBA.

The proposed evolutionary scenario can be investigated further by (1) measuring the evolutionary status of the stellar spheroid and (2) characterising the Mpc-scale environments. How do their molecular gas masses and stellar masses compare with those of SCUBA-selected galaxies (Frayer et al. 1998, 1999; Neri et al. 2003; Greve et al. 2005)? Are they located in over-densities of other luminous star-forming galaxies hosting buried AGN as expected if they are to evolve into cluster elliptical galaxies (e.g. Stevens et al. 2004)? To answer these questions we are now conducting observations of these absorbed QSO fields at submillimetre, mid-infrared and X-ray wavelengths.

ACKNOWLEDGMENTS

The James Clerk Maxwell Telescope is operated by the Joint Astronomy Centre in Hilo, Hawaii on behalf of the parent organizations PPARC in the United Kingdom, the National Research Council of Canada and The Netherlands Organization for Scientific Research. Based on observations obtained with *XMM-Newton*, an ESA science mission with instruments and contributions directly funded by ESA member states and the USA (NASA). We thank the JCMT telescope system specialists for their help, and in particular Jim Hoge for his expertise and energy. J.A.S. thanks PPARC's Rolling Grant Panel for their sagacity. F.J.C. acknowledges support from the Spanish Ministerio de Cienca y Technología, under project ESP2003-00812. I.R.S. acknowledges support from the Royal Society.

REFERENCES

Alexander D.M., et al., 2003, AJ, 125, 383
Alexander D.M., et al., 2004, AJ, submitted
Almaini O., 2003, AN, 324, 109
Almaini O., et al., 2003, MNRAS, 338, 303
Antonucci R., 1993, ARA&A, 31, 473
Archibald E.N., Dunlop J.S., Hughes D.H., Rawlings S., Eales S.A., Ivison R. J., 2001, MNRAS, 323, 417
Barger A., Cowie L.L., Steffen A.T., Hornschemeier A.E., Brandt, W.N., Garmire G.P, 2001, ApJ, 560, L23
Barger A., Cowie L.L., Mushotzsky R.F., Yang Y., Wang W.-H., Steffan A.T., Capak P., 2005, AJ, 129, 578
Baugh C.M., Lacey C.G., Frenk C.S., Granato G.L., Silva L., Bressan A., Benson A.J., Cole S., 2005, MNRAS, 356, 1191
Blain A.W., Longair M.S., 1993, MNRAS, 264, 509
Cash W., 1979, ApJ, 228, 939
Chapman S.C., Blain A.W., Ivison R.J., Smail I.R., 2003, Nat, 422, 695
Chapman S.C., Blain A.W., Smail I., Ivison R.J., 2004, ApJ, in press (astro-ph/0412573)
Devriendt J.E.G., Guiderdoni B., 2000, A&A, 363, 851
Di Matteo T., Springel V., Hernquist L., 2005, Nat, 433, 604
Ellis R.S., et al., 1997, ApJ, 483, 582
Elvis M., et al., 1994, ApJS, 95, 1
Fabian A.C., 1999, MNRAS, 308, L39
Fabian A.C., et al., 2000, MNRAS, 315, 8
Frayer D.T., Ivison R.J., Scoville N.Z., Yun M., Evans A.S., Smail I., Blain A.W., Kneib J.-P., 1998, ApJ, 506, L7
Frayer D.T., et al. 1999, ApJ, 514, L13
Granato G.L., De Zotti G., Silva L., Bressan A., Danese L., 2004, ApJ, 600, 580
Greve T.R., et al., 2005, MNRAS, in press (astro-ph/0503055)
Haas M., Müller S.A.H., Chini R., Meisenheimer, K., Klaas U., Lemke E., Kreysa E., Camezind M., 2000, A&A, 354, 453
Holland W.S., et al., 1999, MNRAS, 303, 659
Hughes D.H., Robson E.I., Dunlop J.S., Gear W.K., 1993, MNRAS, 263, 607
Hughes D.H., et al., 1998, Nat, 394, 241
Isobe T., Feigelson E.D., Nelson P.I., 1986, ApJ, 306, 490
Jenness T., Stevens J.A., Archibald E.N., Economou F., Jessop N.E., Robson E.I., 2002, MNRAS, 336, 14
Kauffmann G. 1996, MNRAS, 281, 487
Kauffmann G., Haehnelt M., 2000, MNRAS, 311, 576
Kennicutt R.C., Jnr., 1998, ApJ, 498, 541

Magorrian J., et al., 1998, AJ, 115, 2285
Mateos S., et al., 2005, A&A, in press (astro-ph/0412390)
McHardy I. M., et al., 2003, MNRAS, 342, 802
McLure R.J., Dunlop J.S., 2002, MNRAS, 331, 795
Mittaz J.P.D., et al., 1999, MNRAS, 308, 233
Neri R., et al., 2003, ApJ, 597, L113
Page M.J., Mittaz J.P.D., Carrera F.J., 2000, MNRAS, 318, 1073
Page M.J., Mittaz J.P.D., Carrera F.J., 2001, MNRAS, 325, 575
Page M.J., Stevens J.A., Mittaz J.P.D., Carrera F.J., 2001, Science, 294, 2516
Page M.J., et al., 2003, AN, 324, 101
Page M.J., Davis S.W., Salvi N.J., 2003, MNRAS, 343, 1241
Page M.J., Stevens J.A., Ivison R.J., Carrera F.J. 2004, ApJ, 611, L85
Priddey R.S., Isaak K.G., McMahon R.G., Omont A., 2003, MNRAS, 339, 1183
Reuland M., Röttgering H., van Breugel W., De Breuck C., 2004, MNRAS, 353, 377
Sandell G., 1994, MNRAS, 271, 75
Silk J., Rees M.J., 1998, A&A, 331, L1
Smail I., Ivison R.J., Blain A.W.,1997, ApJ, 490, L5
Smail I., Scharf C.A., Ivison R.J., Stevens J.A., Bower R.G., Dunlop J.S., 2003, ApJ, 599, 86
Stevens J.A., et al., 2003, Nat, 425, 264
Stevens J.A., Page M.J., Ivison R.J., Smail I.. Carrera F.J., 2004, ApJ, 604, L17
Strüder L., et al., 2001, A&A, 365, L18
Turner M.J.L., et al., 2001, A&A, 365, L27
Waskett T.J., et al., 2003, MNRAS, 341, 1217
Womble D.S., Junkkarinen V.T., Burbidge E.M., 1992, ApJ, 388, 55

This paper has been typeset from a TEX/ LATEX file prepared by the author.